Supporting Information

From Molecule to Nanocrystalline: Ultrafast Dynamics of *Trans-Cis* Isomerization of Azobenzene Derivatives

Jiaxing He [1,2,+], Min Wei [1,+], Ye-Tao Chen [1], David Lee Phillips [2], Li Dang [1,] and Ming-De Li [1,*]*

[1]College of Chemistry and Chemical Engineering, Key (Guangdong-Hong Kong Joint) Laboratory for Preparation and Application of Ordered Structural Materials of Guangdong Province, Shantou University, Guangdong 515063, P. R. China.

[2]Department of Chemistry, The University of Hong Kong, Pokfulam, Hong Kong, China.

+ These authors contributed equally to this work.
* Correspondence to: E-mail: mdli@stu.edu.cn, ldang@stu.edu.cn

Content

A. Material

The chemical reagents used in this work were obtained directly through commercial purchase. Azo-dipyridine (AP) and azobenzene (AB) with 98% purity were purchased from Beijing Bailingwei Technology Co., LTD. Phenylazopyridine (PAP) and diethylamine phenylazopyridine (DAA) with 98% purity were purchased from Shanghai Anaiji Chemical Co., LTD. Spectroscopic grade acetonitrile and spectral hexane were purchased from Beijing Bailingwei Technology Co., LTD. Spectroscopic grade CH3CN and H2O were utilized for the preparation of the sample solutions. All the mixed solvent ratios are volume ratios unless indicated otherwise.

B. Fs-TA Experiments and Kinetics fitting method

The fs-TA setup is based on a Ti: Sapphire regenerative amplified (Coherent, Astrella Tunable-F-1k). The fs-TA spectrometer is Helios Fire mode from Ultrafast Systems. With the 800 nm output power of 7.4 W, the amplifier has a repetition frequency of 1 kHz and the pulse width of 800 nm is 84 fs. The continuous white light is generated from the probe pulse, utilizing approximately 4% of the 800 nm output. The maximum temporal delay of the system is 8000 ps, while the τ_p instrument response function is 120 fs. The recorded data averaged for 2 s is extracted by the acquisition system at each temporal delay.[1] The acetonitrile solution and NCS (0.15 mM) of each sample were removed into a quartz colorimetric dish with a thickness of 2 mm, placed on the sample table, started stirring, excited by pump light of corresponding wavelength (300 uW), and the transmitted detection light signals were collected. The data is stored in a three-dimensional wavelength-time-absorbance matrix. Surface Xplorer is used to analyze all the data, chirp correction is performed on all the data, and solvent effect is deducted. All the error values were shown with 90% confidence intervals. This paper gains the single-wavelength fitting based on Equation (1) below. The t_p and A represent the instrument response value and the amplitude of species, respectively. The t is called delay time, and t_0 means zero time. Meanwhile, in molecular dynamics, normalization can help us more intuitively compare the kinetic behaviors of different molecules or under different conditions. To compare the decay rates between different molecules, we normalize the molecular decay dynamics to the range of [0, 1].

$$S(t) = e^{-(\frac{t-t_0}{t_p})^2} * \sum_i A_i e^{-\frac{t-t_0}{t_i}} \qquad (1)$$

C. The UV absorption spectra evolutions and photoisomerization yields in MeCN.

Under specific LED light irradiation, the ultraviolet absorption spectrum gradually changes from trans-isomer to cis-isomer, and finally reaches equilibrium and stability.

According to the model presented in reference [2], along with the extinction coefficients of AP (24,500 L/mol/cm for the trans-form and 1,500 L/mol/cm for the cis-form, under 280 nm pump), AB (22,700 L/mol/cm for the trans-form and 1,750 L/mol/cm for the cis-form, under 280 nm pump), and PAP (21,800 L/mol/cm for the trans-form and 3,250 L/mol/cm for the cis-form, under 280 nm pump), their respective photoisomerization yields are determined to be 10.5%, 12.5%, and 21.5%.

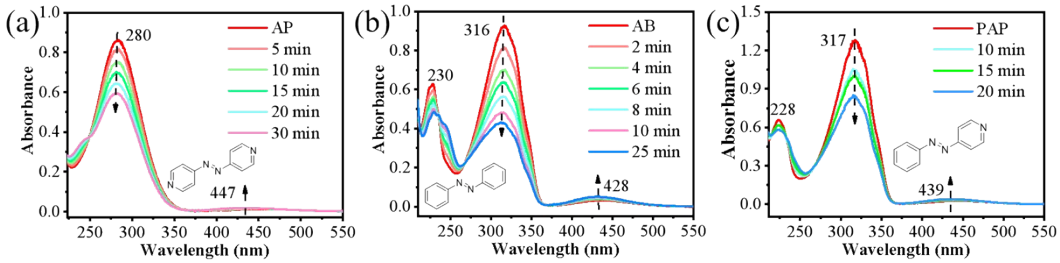

Figure. S1. Shown are the absorption spectra evolutions upon 280 nm laser irradiation of AP in MeCN (a); 300 nm LED light irradiation of AB (b) and PAP (c) in MeCN. The energy density of both the irradiated laser and LED lights on the sample is controlled at 1600 W/m^2.

D. Theoretical Calculations

In this work, Gaussian 16 software is used to complete the theoretical calculations.[3] Using TD-DFT, B3LYP was used as the method and 6-311g** as the basis set to optimize the structure of the ground and excited states of each molecule. Multiwfn[4, 5] program was used to assist analysis of the highest occupied molecular orbital and the lowest unoccupied molecular orbital (HOMO-LUMO, Figure S1) and EDA-FF. All molecules in MeCN were optimized with the SMD model.

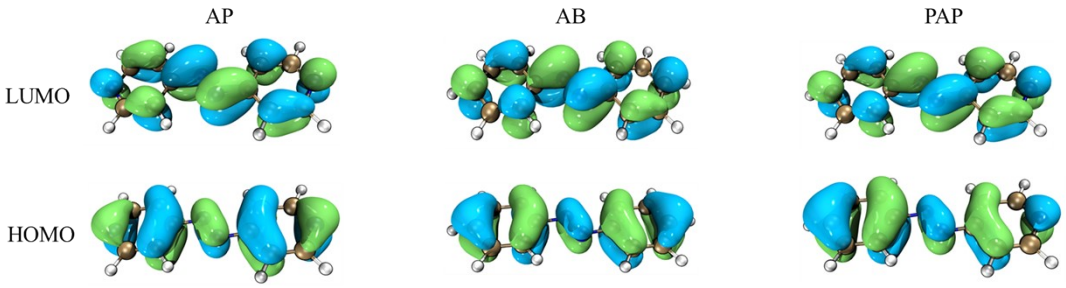

Figure. S2. HOMO-LUMO of azo-derivatives photoswitching molecules.

PES Scanning:

(1) S_0 PES scanning: The PES of each molecular S_0 is scanned. For double-bond photoswitching molecules, the angle formed by two atoms of the double bond and a C atom of the benzene is changed (the angle of C-N=N), and the energy of the S_0 at different angles is optimized to calculate the PES diagram of each azo-derivative *trans*→*cis* isomerization.

(2) S_1 PES scanning: The PES scanning of the S_1 of each azo-derivative is carried out with the dihedral angle where the double bond is located as the independent variable, and the angle of this dihedral angle is changed to optimize the calculation of the energy of the S_1 in different dihedral angle structures (the dihedral of C-N=N-C), and the PES diagram of these molecules occurring in S_1 from *trans* to *cis* isomerization is obtained.

Dipole moment: Molecules have permanent dipole moments (net dipole moment $\boldsymbol{P_0}$, unit: Debye) and induced dipole moments (presented by ***polarizability,*** *a.u.*). The permanent dipole moment is the dipole moment that a molecule generates due to an uneven distribution of charges within it when it is in its equilibrium conformation. Polarizability is the additional dipole moment that a molecule generates when it is deformed by an external electric field. Table S1 shows the relevant data below.

Table S1. The calculated dipole moment and polarizability of azo-derivatives.

	Net Dipole Moment (P_0) (Debye)	Polarizability (α) (a.u.)
AP	0	139.983
AB	0	156.039
PAP	3.058	148.357

E. Compared photoisomerization in MeCN and Hexane

AP, AB and PAP were respectively dissolved in Hexane at a concentration of 0.15 mM for testing fs-TA, then their kinetics and fitting plots were compared with those in MeCN.

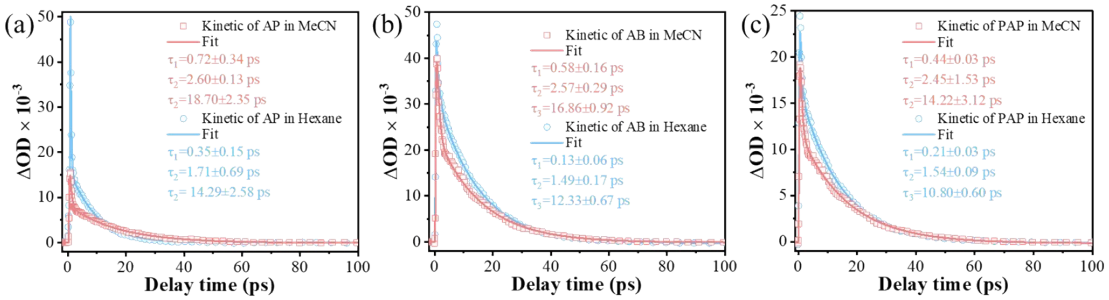

Fig. S3 Compared kinetics and fitting plots of AP (a), AB (b) and PAP (c) in MeCN and Hexane.

F. Preparation of the nanocrystalline suspension

NCS of AP, AB, PAP were prepared by ultrasonic microreactor method.[6] Azo-derivatives were dissolved in CH_3CN solvent, and then high concentration azo-derivatives molecules CH_3CN solution (1.5 mM) and poor solvent water were injected into the ultrasonic microreaction channel at the same time, and a uniformly dispersed nanocrystal suspension (0.15 mM) was obtained by rapid mixing in the ultrasonic-assisted reactor. Detailed parameter: power: 30 W; duration: 5 mL/min; H2O: MeCN=14:1. Then, NCS was filtered by 0.22 μm membrane filter to get nanocrystals. Finally, the obtained nanocrystals were placed in water for ultrasonic dispersion in an ice bath.

G. Characterize the Crystal and Nanocrystal Structure

The size and morphology of azo-derivative nanocrystals were measured by scanning electron microscopy. A small amount of prepared nanocrystalline suspended droplets was absorbed with a rubber head dropper, then added to a 0.5*0.5*0.5 cm silicon wafer and put into the ventilation cabinet for natural air drying to obtain nanocrystalline. Then, the silicon wafer with nanocrystals is plated with a gold film (less than 10 nm). On the one hand, to increase electrical conductivity during the test process, on the other hand, to prevent long-term focus on the damage of organic small molecule crystals, which interferes with the actual particle size detection. The true morphology and particle size of nanocrystals can be determined by scanning electron microscopy and compared with the data obtained by dynamic light scattering test.

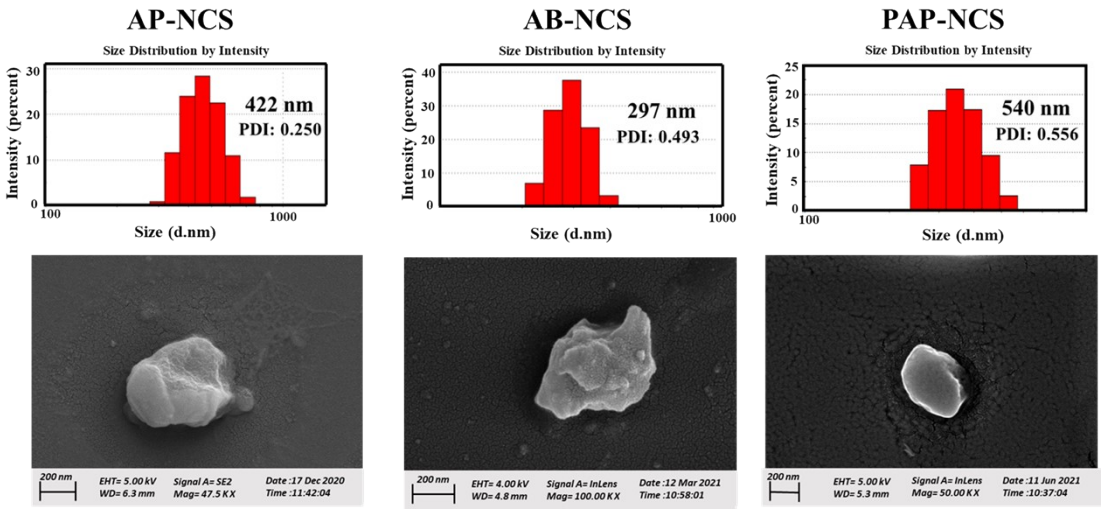

Figure. S4. The DLS and SEM of AP, AB and PAP in NCS.

H. Comparison PXRD of nanocrystal and single crystal

Single crystals of azo-derivatives were prepared by solvent volatilization method, and their crystal structures and intermolecular forces were analyzed by X-ray diffractometer. The nanocrystalline powders were obtained by freeze-drying of the nanocrystalline suspension using a freeze-drying machine. The X-ray powder diffraction spectra of the nanocrystals were measured and compared with the powder X-ray diffraction (PXRD) spectra of the powder made from the single crystals of the corresponding molecules to confirm whether the crystal structure of the nanocrystals is consistent with that of the single crystals (the 2θ Angle range of the test is 5-50°).

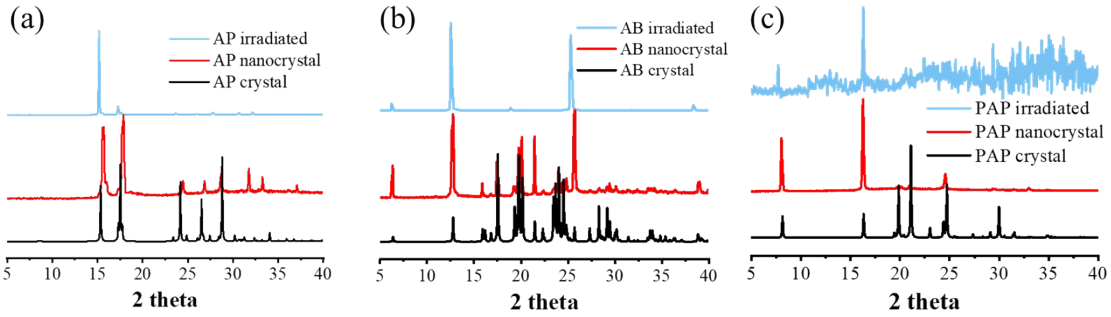

Figure. S5. Comparison PXRD for single crystals (black), nanocrystals (red), and nanocrystals after irradiation 30 min by pumps (blue) of AP (a), AB (b) and PAP (c).

I. The UV absorption spectra evolutions and photoisomerization yields of NCS.

Under specific LED light irradiation, the ultraviolet absorption spectrum gradually changes from trans-isomer to *cis*-isomer and finally reaches equilibrium and stability.

According to the model provided[2], photoisomerization yields of AP, AB and PAP in NCS are 9.6%, 14.2% and 21.2%, respectively.

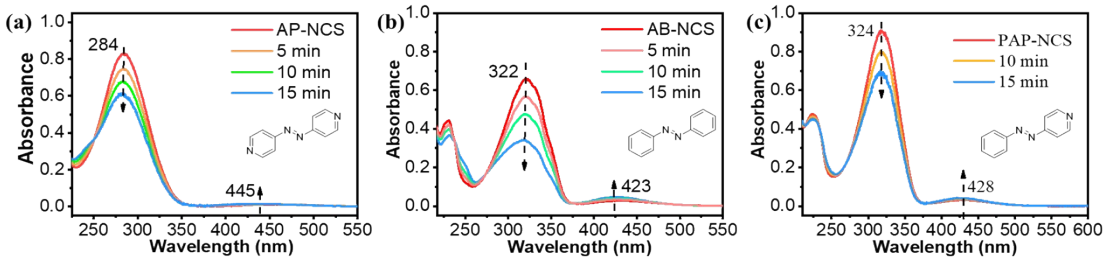

Figure. S6. Shown are the absorption spectra evolutions upon 280 nm laser irradiation of AP in NCS (a); 320 nm laser irradiation of AB in NCS (b); 320 nm laser irradiation of PAP in NCS. The energy density of both the irradiated laser and LED lights on the sample is controlled at 1600 W/m^2.

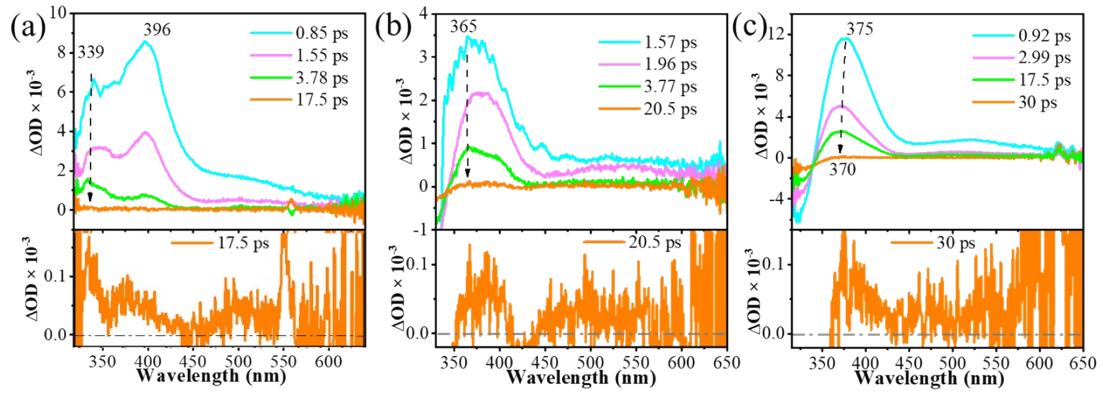

Figure. S7. Fs-TA of AP (a), AB (b), PAP (c) in NCS.

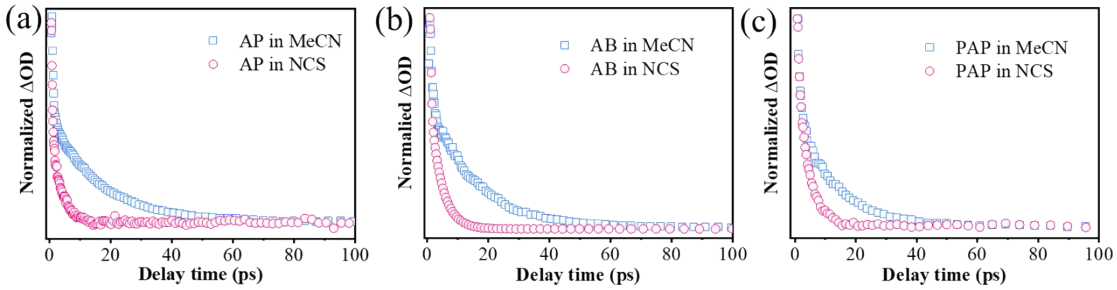

Figure. S8. The respective normalized kinetic comparison of AP (a), AB (b), PAP (c) between in MeCN and NCS.

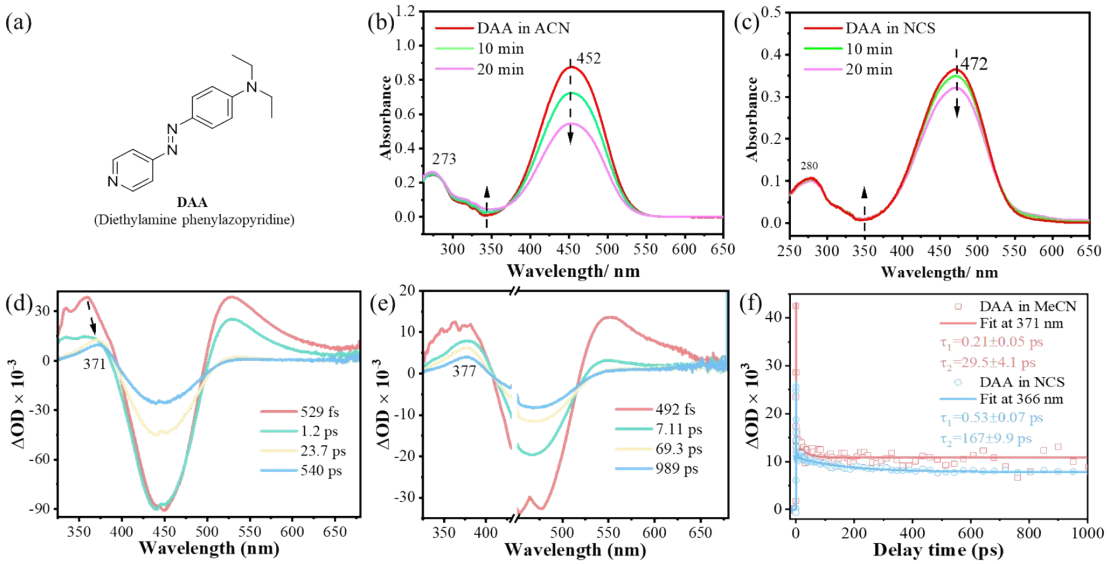

Fig. S9 Shown are the molecular structure of DAA (a), UV-vis absorption spectra evolution of DAA in MeCN (b) and in NCS (c) irradiated by 440 nm LED light, fs-TA spectra of DAA in MeCN (d) and NCS (e) excited by 440 nm pump, and the comparison of kinetic and fitting plots of DAA in MeCN and NCS. The energy density of both the irradiated laser and LED lights on the sample is controlled at 1600 W/m^2.

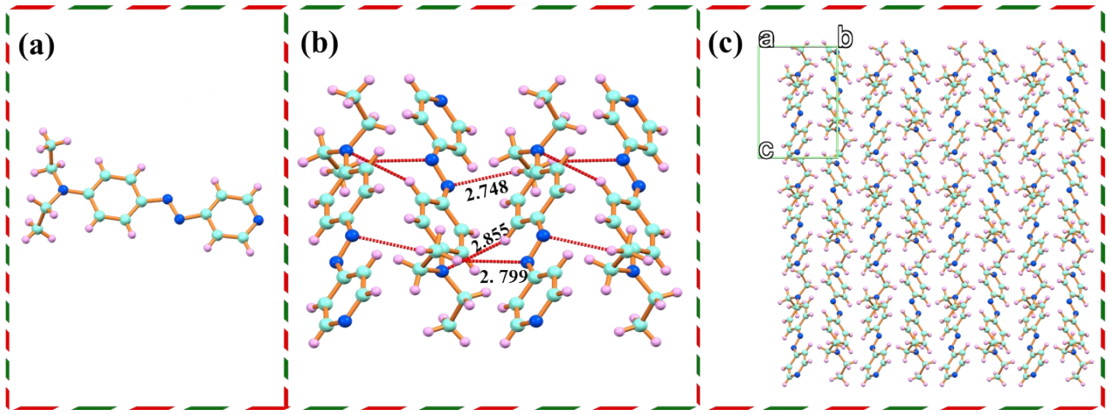

Fig. S10 Single crystal XRD crystal structure of DAA.

J. XYZ coordinates of selected optimized structures

Optimized AP-*trans*-S_0

C	-3.67087	-1.23984	0.
C	-2.28869	-1.10615	0.
C	-1.7635	0.18666	0.
C	-2.63337	1.27085	0.
C	-4.00325	1.01635	0.
H	-4.12093	-2.22949	0.
H	-1.6307	-1.96606	0.
H	-2.23762	2.28001	0.
H	-4.71248	1.84029	0.
N	-0.36955	0.50008	0.
N	0.36955	-0.50008	0.

C	1.7635	-0.18666	0.
C	2.63337	-1.27085	0.
C	2.28869	1.10615	0.
C	4.00325	-1.01635	0.
H	2.23762	-2.28001	0.
C	3.67087	1.23984	0.
H	1.6307	1.96606	0.
H	4.71248	-1.84029	0.
H	4.12093	2.22949	0.
N	4.52484	0.20974	0.
N	-4.52484	-0.20974	0.

Optimized AP-*trans*-S_1

C	1.20786	3.81289	0.00096
C	1.12091	2.43221	0.00115
C	-0.16297	1.84967	0.00004
C	-1.27431	2.71101	-0.00101
C	-1.04539	4.07524	-0.00105
H	2.18803	4.28029	0.00176
H	2.00344	1.80701	0.00205
H	-2.27918	2.3111	-0.00183
H	-1.8909	4.75642	-0.0019
N	-0.34844	0.50314	0.00004
N	0.34844	-0.50314	0.00004
C	0.16297	-1.84967	0.00004
C	1.27431	-2.71101	-0.00101
C	-1.12091	-2.43221	0.00115
C	1.04539	-4.07524	-0.00105
H	2.27918	-2.3111	-0.00183
C	-1.20786	-3.81289	0.00096
H	-2.00344	-1.80701	0.00205
H	1.8909	-4.75642	-0.0019
H	-2.18803	-4.28029	0.00176
N	-0.16297	-4.64295	-0.00011
N	0.16297	4.64295	-0.00011

Optimized AP-CI-S_1

C	-3.39484	1.21361	0.68825
C	-2.10201	1.0742	0.20362
C	-1.7506	-0.15328	-0.36777
C	-2.70804	-1.16818	-0.42388
C	-3.96343	-0.90636	0.10145
H	-3.69912	2.15417	1.1372
H	-1.38593	1.88382	0.25179

H	-2.46644	-2.12579	-0.86546
H	-4.72785	-1.67645	0.07715
C	1.51053	0.46881	0.02908
C	1.59202	-0.40486	1.1184
C	2.50357	1.43712	-0.13265
C	2.66555	-0.25682	1.98522
H	0.84399	-1.17263	1.26518
C	3.52172	1.48635	0.80619
H	2.46944	2.12274	-0.9688
H	2.75776	-0.91947	2.84033
H	4.30614	2.23031	0.71032
N	-0.49484	-0.37594	-0.90946
N	0.49484	0.37713	-0.90898
N	3.62007	0.66325	1.85213
N	-4.32096	0.25639	0.65037

Optimized AB-*trans*-S_0

C	-1.36183	3.63175	-0.00001
C	-0.61916	2.46232	0.
C	-1.27945	1.231	0.00001
C	-2.67059	1.17979	0.00001
C	-3.41017	2.35627	0.
C	-2.75614	3.58262	-0.00001
H	-0.85605	4.58986	-0.00002
H	0.46238	2.47708	0.
H	-3.14771	0.20731	0.00001
H	-4.49248	2.31577	0.
H	-3.32896	4.50222	-0.00002
C	1.27945	-1.231	0.00001
C	0.61916	-2.46232	0.
C	2.67059	-1.17979	0.00001
C	1.36183	-3.63175	-0.00001
H	-0.46238	-2.47708	0.
C	3.41017	-2.35627	0.
H	3.14771	-0.20731	0.00001
C	2.75614	-3.58262	-0.00001
H	0.85605	-4.58986	-0.00002
H	4.49248	-2.31577	0.
H	3.32896	-4.50222	-0.00002
N	-0.61916	-0.0315	0.00001
N	0.61916	0.0315	0.00001

Optimized AB-*trans*-S_1

C	-1.36183	3.63175	-0.00001

C	-0.61916	2.46232	0.
C	-1.27945	1.231	0.00001
C	-2.67059	1.17979	0.00001
C	-3.41017	2.35627	0.
C	-2.75614	3.58262	-0.00001
H	-0.85605	4.58986	-0.00002
H	0.46238	2.47708	0.
H	-3.14771	0.20731	0.00001
H	-4.49248	2.31577	0.
H	-3.32896	4.50222	-0.00002
C	1.27945	-1.231	0.00001
C	0.61916	-2.46232	0.
C	2.67059	-1.17979	0.00001
C	1.36183	-3.63175	-0.00001
H	-0.46238	-2.47708	0.
C	3.41017	-2.35627	0.
H	3.14771	-0.20731	0.00001
C	2.75614	-3.58262	-0.00001
H	0.85605	-4.58986	-0.00002
H	4.49248	-2.31577	0.
H	3.32896	-4.50222	-0.00002
N	-0.61916	-0.0315	0.00001
N	0.61916	0.0315	0.00001

Optimized AB-CI-S_1

C	-2.62579	-1.16401	1.15279
C	-1.54245	-0.32827	0.97564
C	-1.56027	0.63361	-0.07099
C	-2.70959	0.73001	-0.90013
C	-3.77877	-0.11599	-0.70447
C	-3.74385	-1.06841	0.31965
H	-2.61188	-1.89849	1.94892
H	-0.67906	-0.38692	1.62486
H	-2.7035	1.47925	-1.68142
H	-4.65032	-0.04228	-1.34319
H	-4.58765	-1.72986	0.4715
C	1.5638	0.63502	0.09103
C	1.55238	-0.27826	-0.99034
C	2.70172	0.69655	0.92869
C	2.63911	-1.10946	-1.19625
H	0.6944	-0.30934	-1.64929
C	3.7724	-0.1443	0.70714
H	2.69406	1.41304	1.74041
C	3.74869	-1.05434	-0.35392

H	2.62747	-1.80641	-2.02585
H	4.63712	-0.09615	1.35787
H	4.59272	-1.7106	-0.52501
N	-0.5404	1.46956	-0.34911
N	0.52359	1.45828	0.39599

Optimized PAP-*trans*-S_0

C	3.66689	1.24406	0.00001
C	2.28765	1.09938	0.
C	1.76948	-0.19442	-0.00001
C	2.64864	-1.26886	-0.00001
C	4.0148	-1.00553	0.
H	4.10872	2.23554	0.00002
H	1.62572	1.95378	0.
H	2.2612	-2.27949	-0.00001
H	4.72878	-1.82311	0.
C	-1.75841	0.17706	-0.00001
C	-2.28238	-1.11839	0.
C	-2.60577	1.28154	-0.00001
C	-3.65629	-1.29327	0.00001
H	-1.60297	-1.96001	0.
C	-3.98325	1.09915	0.
H	-2.16192	2.26958	-0.00001
C	-4.508	-0.18784	0.00001
H	-4.07126	-2.29392	0.00002
H	-4.64374	1.95733	0.
H	-5.58145	-0.33441	0.00002
N	0.37838	-0.51529	-0.00002
N	-0.36655	0.47555	-0.00002
N	4.52769	0.22223	0.00001

Optimized PAP-*trans*-S_1

C	-3.81236	-1.21783	0.00006
C	-2.43055	-1.12649	0.00001
C	-1.86563	0.16386	-0.00003
C	-2.73312	1.2733	-0.00006
C	-4.09295	1.02647	0.00001
H	-4.26688	-2.2065	0.00009
H	-1.80597	-2.00741	-0.00001
H	-2.35011	2.28306	-0.00013
H	-4.77897	1.87051	-0.00001
C	1.86452	-0.16389	-0.00004
C	2.40374	1.13366	0.00003
C	2.71025	-1.28486	-0.00005

C	3.78105	1.28616	0.00006
H	1.73955	1.98778	0.00005
C	4.0812	-1.09774	0.
H	2.28059	-2.27808	-0.00008
C	4.62917	0.18321	0.00004
H	4.19489	2.28728	0.00011
H	4.73097	-1.96435	-0.00001
H	5.70271	0.31934	0.00007
N	-0.52653	0.34044	-0.00006
N	0.50916	-0.34831	-0.00006
N	-4.64816	-0.18452	0.00007

Optimized PAP-CI-S_1

C	0.0107	2.66407	-2.92266
C	-0.20739	1.60922	-2.05117
C	0.57733	1.50557	-0.88846
C	1.56768	2.46378	-0.62163
C	1.76429	3.50718	-1.5092
C	0.99128	3.61761	-2.66374
H	-0.59605	2.74029	-3.81737
H	-0.96678	0.86235	-2.2424
H	2.16324	2.37024	0.27722
H	2.53012	4.24389	-1.29816
H	1.15186	4.43693	-3.35244
C	-0.28768	-1.74457	-0.51294
C	0.87612	-2.161	-1.18419
C	-1.36502	-2.63099	-0.35889
C	0.94216	-3.45029	-1.68732
H	1.69786	-1.46557	-1.29459
C	-1.27226	-3.91316	-0.8713
H	-2.25364	-2.29565	0.16002
H	1.84062	-3.76721	-2.20385
H	-2.1069	-4.5931	-0.74946
N	0.39521	0.47897	-0.00005
N	-0.39521	-0.47897	-0.00005
N	-0.12284	-4.33418	-1.53784

Reference

1. J. H. Pang, J. X. He, Z. Q. Deng, W. B. Chen, S. L. Chen, S. F. Ni, D. L. Phillips, Z. Y. Dong, L. Dang, M. D. Li, *Adv. Opt. Mater.,* 2023, **11**, 16.

2. K. Stranius, K. Börjesson, *Sci. Rep.,* 2017, **7**, 41145.

3. M. J. Frisch, G. W. Trucks, H. B. Schlegel, G. E. Scuseria, M. A. Robb, J. R. Cheeseman, G. Scalmani, V. Barone, G. A. Petersson, H. Nakatsuji, X. Li, M. Caricato, A. V. Marenich, J. Bloino, B. G. Janesko, R. Gomperts, B. Mennucci, H. P. Hratchian, J. V. Ortiz, A. F. Izmaylov, J. L. Sonnenberg, Williams, F. Ding, F. Lipparini, F. Egidi, J. Goings, B. Peng, A. Petrone, T. Henderson, D. Ranasinghe, V. G. Zakrzewski, J. Gao, N. Rega, G. Zheng, W. Liang, M. Hada, M. Ehara, K. Toyota, R. Fukuda, J. Hasegawa, M. Ishida, T. Nakajima, Y. Honda, O. Kitao, H. Nakai, T. Vreven, K. Throssell, J. A. Montgomery Jr., J. E. Peralta, F. Ogliaro, M. J. Bearpark, J. J. Heyd, E. N. Brothers, K. N. Kudin, V. N. Staroverov, T. A. Keith, R. Kobayashi, J. Normand, K. Raghavachari, A. P. Rendell, J. C. Burant, S. S. Iyengar, J. Tomasi, M. Cossi, J. M. Millam, M. Klene, C. Adamo, R. Cammi, J. W. Ochterski, R. L. Martin, K. Morokuma, O. Farkas, J. B. Foresman, D. J. Fox, Gaussian 16 *Rev. C.*01, Wallingford, CT, 2016.

4. Z. Dong, S. D. A. Zondag, M. Schmid, Z. Wen, T. Noël, *Chem. Eng. J*. 2022, **428**, 130968.

5. T. Lu, F. Chen, *J. Comput. Chem.,* 2012, **33***,* 580-592.

6. T. Lu, *J. Comput. Chem.,* 2024, **161***,* 082503.